Deltares

WTI 2017: Toetsregel Piping

Piping and transient groundwater flow

dr.ir. J.M. van Esch

1209435-003

Deltares

Title
WTI 2017: Toetsregel Piping

Client	Project	Reference	Pages
Rijkswaterstaat	1209435-003	1209435-003-GEO-0005	20

Trefwoorden
Finite element method, Groundwater flow, Piping Dikes Dams

Samenvatting
Dikes and dams are water mitigating structures that protect the land from floods and high tides. In the Netherlands these structures are often constructed of impervious clays and are built on a sandy aquifer as subsoil. Foundations of such geotechnical structures are vulnerable to an erosion effect called piping that refers to the development of small flow channels that begin at the downstream side of the structure where the seepage pressure is high. The internal erosion process works its way to the upstream side, and if the erosion process continues the structure may collapse. Failure due to piping is a risk for many river levee systems. In the Netherlands, piping is the dominant failure mechanism. The prediction of this phenomenon has therefore received much attention in the past and is still being investigated. Starting with simple empirical rules in the beginning of previous century, with ongoing research the prediction models have become more physics based, and are often founded or calibrated using experimental data. However, the current model of Sellmeijer does not describe the hole piping process sufficiently. These deficiencies gave reason to develop the finite element groundwater flow model DgFlow. This enables modeling of all erosion processes concerning piping in one tool, taking into account effects like time-dependent loads and heterogeneity of the subsoil. This report verifies DgFlow against Sellmeijer's rule for a simplified dam on a homogeneous subsurface for which the rule was designed. Two multilayer subsurface configurations are examined next and the results compare well with the outcome of the steady state groundwater simulator MSeep. A series of model simulations then identifies the effect of phreatic storage and elastic storage on the time dependent development of groundwater pressures. The delay due to storage hampers the growth of the piping channel. The applicability of the model for more realistic cases is investigated by considering a simplified river dike and a sea defense. In future a number of well instrumented cases will be considered.

Versie	Datum	Auteur	Paraaf	Review	Paraaf	Goedkeuring	Paraaf
1	nov. 2014	dr.ir. J.M. van Esch		ir. V.M. van Beek		ir. L. Voogt	

State
final

Deltares

Title
WTI 2017: Toetsregel Piping

Client	Project	Reference	Pages
Rijkswaterstaat	1209435-003	1209435-003-GEO-0005	20

Contents

1 Introduction

In delta regions dikes protect the land from floods and high tides. In the Netherlands dikes are generally constructed of impervious clays and are built on a sandy aquifer as subsoil. The foundations of these geotechnical structures are vulnerable to an erosion process called piping. Piping is a form of seepage erosion where groundwater flow affects the soil stability. In literature, the piping mechanism is also referred to as backward erosion or underseepage erosion (Lane (1935); Wolfs (2002)). Figure 1.1 illustrates the piping process for a cross section of a dike on a low permeability holocene layer, which covers a pleistocene high permeability aquifer.

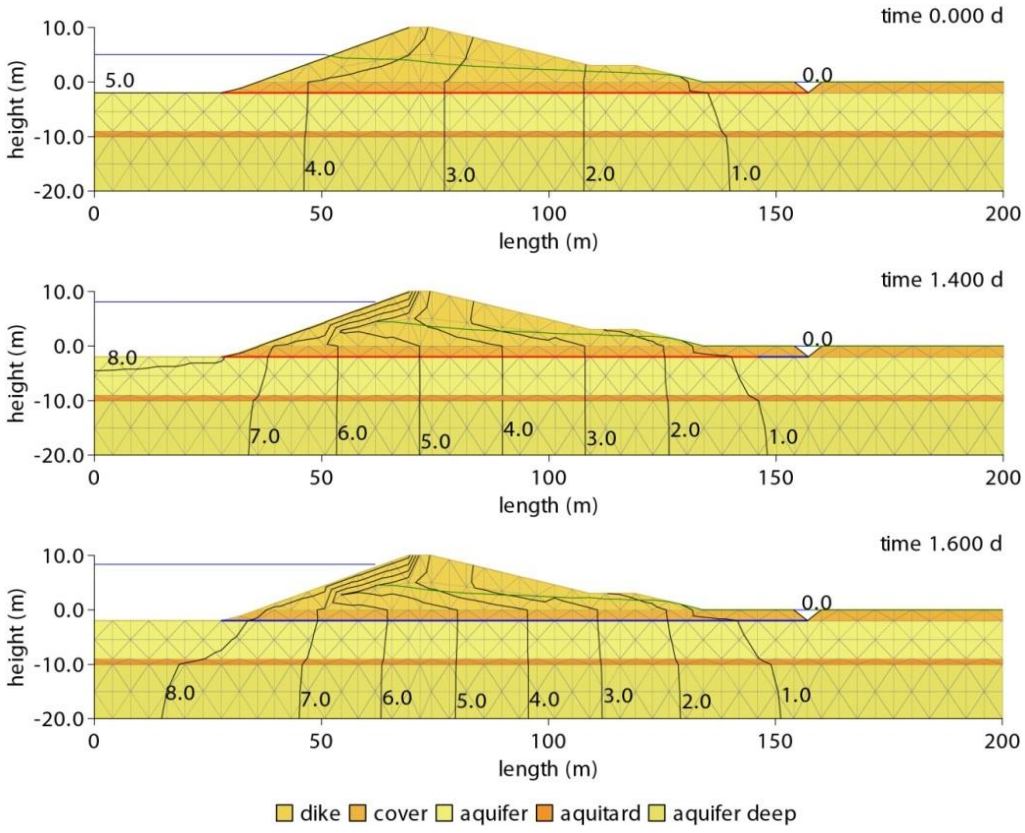

Figure 1.1 Piping under a dike, indicated by the blue line at the base of the embankment.

The blue line displays the free water level at the river side, and the green line presents the phreatic surface in the dike. In this configuration seepage occurs at the lower end of the berm, where the green line intersects the dike surface. The black lines present the decline of

the hydraulic head in the aquifer from the river side to the polder. The top picture shows the initial situation where, given the head difference over the structure, there is no piping channel under the dike. This is indicated by the red line at the base of the structure. The middle picture shows a stable active piping channel of 12 meters due to the increased head difference over the structure. The active piping channel is indicated by the blue part of the base line. The bottom picture finally shows a piping channel that extends to the upstream side. This situation was obtained for a head difference that exceeds the critical head difference related to the piping mechanism.

For the piping mechanism four phases can be distinguished; the initiation phase, the equilibrium phase, the progressive phase, and the widening phase. The initiation phase starts the process. If the water pressure underneath the cover layer exceeds the weight of the cover layer then uplift conditions apply, the cover layer might crack and preferential flow lines will develop through the subsoil. This will start a concentrated groundwater flux and small sand boils at the downstream exit point will develop. This initial phase is also known as the boiling phase where sand boils without the deposition of sand. Further increase of head leads to pipe formation causing the sand boils to transport and deposit sand. In the equilibrium phase small channels that begin at the sand boils, where the seepage pressure is high, develop towards the upstream side and the sand boils grow as more material is transported out of the subsurface. In this phase of the process the erosion channel has a finite length smaller than the construction length and grains in the channels are in equilibrium. If the head difference over the structure increases then the propagation of erosion channels continues and the small channels grow in size. In the progression phase the pipe develops towards the upstream side. At the moment the piping channel reaches the upstream side the material transport strongly increases. This is known as the widening phase. Finally the structure may collapse and then water overflows the dike.

Failure due to piping is a risk for many river levee systems. The prediction of this phenomenon has therefore received much attention in the past and is still being investigated. Starting with simple empirical rules in the beginning of previous century, with ongoing research the prediction models have become more physics based, and are often founded or calibrated using experimental data. In the Netherlands these prediction models are used to perform a 12-yearly safety assessment of primary water-retaining structures. To perform the safety assessment, an assessment protocol (WTI) is determined by the secretary of Infrastructure and the environment, consisting of the Voorschrift Toetsen op Veiligheid (VTV) and Hydraulische Randvoorwaarden (HR). At present the most advanced design rule for

piping is the rule proposed by Sellmeijer (1988). This rule is based on the analysis of the mechanism under an impervious structure of base length L (m) on top of a single aquifer of constant height D (m). Sellmeijer's rule predicts the critical head difference H_c (m) between the outer river water level at one side of the structure and polder water level to the other side of the structure. If the actual head difference is larger than the critical head difference, a piping channel will propagate until the channel reaches the upstream side. The rule in the current form as proposed by Sellmeijer et al. (2011), is given by

$$H_c = F_r F_s F_g L, \tag{1.1}$$

where F_r (-) expresses the resistance term, F_s (-) denotes the scaling term, and F_g (-) expresses the geometry term, in which

$$F_r = \frac{\rho^s - \rho^l}{\rho^l}\eta \tan\vartheta, \quad F_s = \frac{d_{70}}{\sqrt[3]{\kappa L}}, \quad F_g = 0.91\left(\frac{D}{L}\right)^{\varsigma}, \quad \varsigma = \frac{0.24}{\left(\frac{D}{L}\right)^{2.8} - 1}. \tag{1.2}$$

In the expression of the resistance term ρ^s $(\mathrm{kg/m^3})$ corresponds to the density of the soil particles, ρ^l $(\mathrm{kg/m^3})$ denotes the density of the water phase, η (-) expresses White's constant, and ϑ (deg) is the bedding angle. The scaling term includes the intrinsic permeability κ $(\mathrm{m^2})$ of the sand under the structure, the 70 grain diameter d_{70} (m) and the potential piping length. The coefficient ς (-) has a value of 1.08 for $D/L = 1$ as follows from a limit analysis. The geometry term relates the thickness of the aquifer to the potential piping length and includes a coefficient 0.91, which was determined using numerical modeling. According to Sellmeijer's rule larger values of L, ρ^s, η, ϑ, d_{70}, and smaller values for D, κ and ρ^l increase the critical head difference H_c and reduce the risk of piping.

To improve prediction models for increased safety and optimal reinforcement of levees, the research program SBW (Strength and loads on Flood defense structures) has been initiated as he current model of Sellmeijer does not describe the hole piping process sufficiently. These deficiencies gave reason to develop the finite element groundwater flow model DgFlow. This enables modeling of all erosion processes concerning piping in one tool, taking into account effects like time-dependent loads and heterogeneity of the subsoil. DgFlow was

developed as part of the safety assessment program (WTI2017), which is funded by the Rijkswaterstaat; the executive arm of the Dutch Ministry of Infrastructure and the Environment.

Chapter 2 outlines the mathematical model that forms the basis of the groundwater flow simulator DgFlow. Van Esch ea. (2013a) presented the numerical algorithm for solving this mathematical model. Chapter 3 verifies DgFlow against Sellmeijer's rule for a simplified dam on a homogeneous subsurface for which the rule was designed. Two multilayer subsurface configurations are examined next and the results compare well with the outcome of the steady state groundwater simulator MSeep. A series of model simulations then identifies the effect of phreatic storage and elastic storage on the time dependent development of groundwater pressures. The delay due to storage hampers the growth of the piping channel. The applicability of the model for more realistic cases is investigated by considering a simplified river dike and a sea defense. In future a number of well instrumented cases will be considered. Chapter 4 draws the conclusions.

2 Numerical model

Sellmeijer's rule, as presented by Sellmeijer ea. (2011), adopts equilibrium of forces as suggested by White (1940) and assumes laminar flow around the grains. Transport of grains takes place at the bottom of the pipe as long as the grains are not in equilibrium, when the pipe becomes deeper and longer. This process is known as secondary erosion.

Grain equilibrium

Sellmeijer's model applies a single particle approach for which the transport equations consider equilibrium of forces. The forces that are taken into account are the gravitational force and the drag force. The force due to the vertical hydraulic gradient and the force due to the horizontal gradient are neglected.

The grain is at rest if the drag force does not exceed the counteracting gravitational force. This is the case if the shear stress exerted by the water is less than the critical shear stress $\tau_c \quad (\mathrm{N/m^2})$, which reads

$$\tau_c = \frac{\pi}{6}\left(\rho^s - \rho^l\right) g \eta d_c \tan\vartheta \tag{2.1}$$

Here $\rho^s \quad (\mathrm{kg/m^3})$ corresponds to the density of the soil particles, $\rho^l \quad (\mathrm{kg/m^3})$ denotes the density of the water phase, $\eta \quad$ (-) expresses White's constant, $\vartheta \quad (\mathrm{deg})$ is the bedding angle, and d_c (m) denotes a characteristic grain diameter. The bedding angle ϑ approximately represents the maximum slope of a pile of grains under water. White's parameter η was set to 0.25 and accounts for the uptake of shear stress of a single particle in a sand bed. For larger values of the shear force, its component parallel to the grain interface will be larger than the gravitational force in that direction and the particle will move.

The actual shear stress exerted by the water depends on the height of the channel $a \quad (m)$ and the pressure gradient along the pipe. This shear stress can be expressed as

$$\tau = \frac{a}{2}\frac{dp}{dx} \tag{2.2}$$

A combination of Equations (2.1) and (2.2) specifies the limit state equilibrium according to

$$a\frac{dp}{dx}=\frac{\pi}{3}\left(\rho^{s}-\rho^{l}\right)\eta d_{c}\tan\vartheta \tag{2.3}$$

Subsurface flow equation

Flow through a partly saturated porous medium can be modeled considering conservation of mass and a generalization of Darcy's law, which can be written as

$$\left(\alpha+n\beta\right)S\frac{\partial p}{\partial t}+n\frac{dS}{dp}\frac{\partial p}{\partial t}+\frac{\partial q_{i}}{\partial x_{i}}=0\,,\quad q_{i}=-\frac{k_{r}\kappa_{ij}}{\mu^{l}}\left(\frac{\partial p}{\partial x_{j}}-\rho^{l}g_{j}\right)\quad\text{on}\quad\Omega^{p}\,, \tag{2.4}$$

where α $(\mathrm{m}^2/\mathrm{N})$ is the compressibility of the soil skeleton, β $(\mathrm{m}^2/\mathrm{N})$ represents the compressibility of the pore water, n (-) denotes porosity and S (-) expresses the degree of saturation of the liquid phase in the void space. The compressibility in the case of elastic behavior of the soil skeleton can be written as $\alpha=1/(\lambda+2\nu)$, where λ $(\mathrm{N}/\mathrm{m}^2)$ and ν $(\mathrm{N}/\mathrm{m}^2)$ denote Lamè's constants. Specific discharge q_i (m/s) relates to relative permeability k_r (-), intrinsic permeability κ_{ij} (m^2), dynamic viscosity of the liquid phase μ^l $(\mathrm{kg}/\mathrm{ms})$ and its density ρ^l $(\mathrm{kg}/\mathrm{m}^3)$. For a y-coordinate pointing in the opposite direction than the gravitational vector g_y is $-9.81\mathrm{m}/\mathrm{s}^2$. Equation (2.4) is known as the storage equation.

Constitutive equations for the degree of saturation of a fluid in a porous medium are based on the capillary pressure. The capillary pressure denotes the difference of the non-wetting and the wetting phase pressure. For liquid-gas flow systems the liquid phase is the wetting phase and the gas phase is the non-wetting phase. The capillary pressure p_c $(\mathrm{N}/\mathrm{m}^2)$ reads $p_c=p^g-p^l$. If the gas phase is stagnant, the pressure in the gas phase is constant and equals the atmospheric pressure if the phase is continuous. Then, $p_c=-p^l$ holds for unsaturated conditions and $p_c=0$ applies for saturated conditions. Van Genuchten and Brooks-Corey (Aziz and Settari, 2002) simplified this by an empirical relation $p_c=p_c\left(S\right)$,

where S denotes the saturation of the wetting phase, as can be found in Vogel et al. (2001); Aziz and Settari (2002). Reversely, Van Genuchten-Mualem expresses the saturation as a functional relation of wetting phase pressure according to $S = S(p)$. The Van Genuchten model is written as

$$S = S_r + (S_s - S_r)\left[1 + |g_a \psi|^{g_n}\right]^{-g_m} \quad \text{if} \quad \psi < \psi_a, \qquad S = S_s \quad \text{for} \quad \psi \geq \psi_a, \qquad (2.5)$$

where ψ (m) denotes the pressure head, which reads $\psi = p^l / \rho^l g$, ψ_a (m) is the air-entry pressure head, which is constrained by $\psi_a \leq 0$. S_r (-) is the minimal saturation and S_s (-) denotes the maximum degree of saturation. The minimal saturation deviates from zero due to chemically attached water or entrapped water pockets. The maximum degree of saturation is less than one mainly as a result of entrapped air. The Van Genuchten relation counts two empirical shape factors that have to be measured in the laboratory: g_n (-), and g_a $(1/\mathrm{m})$. For convenience a third shape factor g_m (-) was introduced as $g_m = (g_n - 1)/g_n$.

Mualem-Van Genuchten and Brooks-Corey proposed empirical relations for the relative permeability, which can be found in Vogel et al (2001); Aziz and Settari (2002). The Van Genuchten relation reads

$$k_r = (S_e)^{g_l}\left[1 - \left(1 - S_e^{1/g_m}\right)^{g_m}\right]^2, \qquad S_e = \frac{S - S_r}{S_s - S_r}, \qquad (2.6)$$

where the empirical shape factor g_l (-) is often set to 0.5. DgFlow adopts the Van Genuchten model because this model is generally used in engineering practice. However the material parameters of the model need to be measured in the laboratory. This is mostly done on small scale samples and the model does not apply for macro scale field problems that involve structured soils. An up-scaling procedure or a double porosity approach could solve this mismatch of scales.

Two types of boundary conditions complete the problem definition; Dirichlet conditions prescribe the pressure on parts of the boundary and Von Neumann boundary conditions

prescribe the derivative of the pressure or flux on the boundary. These first-type and second-type boundary conditions read

$$p = \bar{p} \quad \text{on} \quad \Gamma_1^p, \quad q_i n_i = -\bar{q} \quad \text{on} \quad \Gamma_2^p, \quad q_i n_i = -s \quad \text{on} \quad \Gamma_3^p, \tag{2.7}$$

where Γ_1^p, Γ_2^p and Γ_3^p are disjoint parts of the boundary where the conditions apply, n_i $(-)$ denotes the outward pointing normal to the boundary, $\bar{p}$ $(\mathrm{N/m^2})$ is the prescribed pressure, $\bar{q}$ $(\mathrm{m/s})$ denotes the volumetric water flux over the boundary into the flow domain as a source term, and s $(\mathrm{m/s})$ expresses a source term that will be used for coupling the subsurface flow equation to the flow equation for piping. In the current implementation these boundary conditions are generalized to seepage conditions where outflow only occurs under saturated conditions and inflow is prevented. Seepage conditions in turn can be extended to submerging conditions where free water level variations are taken into account, infiltration conditions that simulate precipitation and over-topping conditions, and evaporation conditions.

Pipe flow equation

Poiseuille flow through a horizontal slit can be written as

$$v = -\frac{a^2}{12\mu}\frac{dp}{dx}, \tag{2.8}$$

where a (m) denotes the height of the channel. The total flow through a rectangular duct then follows from multiplication by the height of the channel as $q = av$ for a two dimensional case. If flow through a small channel is modeled in one dimension (within a 2D flow domain) then the flow equation through for the pipes follows from the application of conservation of mass and Poiseuille flow as

$$\frac{dq}{dx} + s = 0, \quad q = -\frac{a^3}{12\mu}\frac{dp}{dx} \quad \text{on} \quad \Omega^c, \tag{2.9}$$

In this equation s $(1/\mathrm{s})$ expresses a sink term (Huyakorn and Pinder (1983)) and an artificial permeability $\kappa^* = a^3/12$ could be used to transform the Poisseuille flow into Darcy flow.

Here the extension of the pipe flow domain Ω^c (m) corresponds to the boundary of the subsurface flow domain Γ^p (m) as equation (2.9) holds for a one-dimensional flow domain. Dirichlet conditions hold on the inflow and outflow point of the piping domain. Boundary conditions for the piping domain are given by

$$p = \overline{p} \quad \text{on} \quad \Gamma_1^c . \tag{2.10}$$

The condition of limit equilibrium for the horizontally oriented erosion channel according to Sellmeijer (1988) reads

$$a\frac{dp}{dx} = \frac{\pi}{3}\left(\rho^s - \rho^l\right) g d_{70} \eta \tan\vartheta . \tag{2.11}$$

The height of the erosion channel varies between 0 and 3 grains in an experimental setup, 0 to 10 grains in a field test and 0 to 30 grains for an embankment.

The set of equations given by (2.4) and (2.9) and closed by equation (2.7) and (2.10) is solved numerically (Van Esch ea., 2013a). The piping elements are sorted in upstream direction and an active length is attached to all elements. The active length of the elements is set to zero at the start of a computation as $\Delta x_i = 0$, where $i = 1 \ldots n$, and n denotes the number of elements. Within a simulation the piping algorithm checks the equilibrium conditions first for the element near the exit point. If the limit equilibrium condition (2.11) is satisfied for this element then the velocity within the element follows from equation (2.8). If the active length $\Delta x_1 = v_1 \Delta t$ within a time step Δt exceeds the actual length of the element for $\Delta x_1 \geq l_1$ then the element is activated and the adjacent element in upstream direction is checked. For this element the active length follows from $\Delta x_2 = v_2\left(\Delta t - \Delta t_1\right)$, where $\Delta t_1 = \Delta x_1 / v_1$. If this element cannot be activated in this time step then its active length is increased within the next time step for which the equilibrium condition is met and the active length is compared with the element length. This process is repeated throughout the entire simulation.

3 Numerical simulations

This chapter presents four benchmark problems that compare the outcome of DgFlow simulation with either Sellmeijer's rule that holds for a single layered subsurface or with MSeep simulation results. MSeep considers multi-layered systems and steady state groundwater flow. A series of DgFlow simulations then address the effect of transient groundwater flow due to an increase in the free water level in time, which provides a hydraulic load on the system. The rate of water level change relates to the load on a river dike or a more rapid load on a sea defence. The applicability of the model for more realistic cases is investigated by considering a simplified river dike and a sea defense.

3.1 Benchmark problems

Figure 3.1 shows the layout of a simplified dam geometry with a low permeable structure that is supported by an aquifer of high permeability, as well as the finite element mesh used for the flow simulation. To the left side of the structure the water level imposes a hydraulic head condition on the horizontal edge of the aquifer and to the right side of the structure a constant water level applies. The vertical boundaries and base of the aquifer are considered impervious. Submerging seepage face boundary conditions apply on the external dam boundaries. The structure itself has a low permeability. Thus, water flows under the structure through the aquifer from the river side towards the polder and to hardly any water flows through the structure. Sellmeijer (2011) considered an impermeable structure on top of an aquifer with the same hydraulic loading conditions.

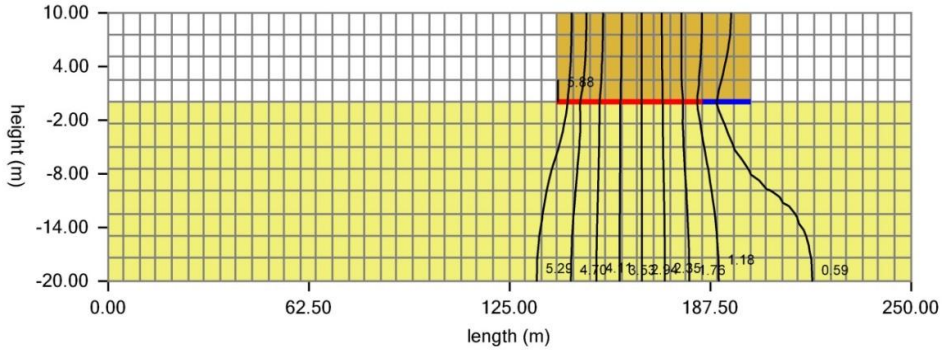

Figure 3.1 Structure on a sandy subsurface.

The numerical experiments outlined in this section consider a set microscale material parameters; the particle diameter is 0.1 mm, the density of the grains equals $2.65 \cdot 10^3 \, \mathrm{kg/m^3}$;

White's constant is 0.25 and bedding angle that is assumed to be 37 deg. The geometry of the problem is given by the thickness of the aquifer of 20 meters and the potential piping length of 60 meters. The solid skeleton has an hydraulic permeability of 1 m/d. The pore water has a unit weight of 10 kN/m^3 and dynamic viscosity of $10^{-3}\,\mathrm{Ns/m^2}$. The gravitational acceleration is set to10 m/s^2.

Figure 3.1 shows the result of a steady state groundwater flow computation where the piping channel did not reach the upstream side and its length remains stable for the imposed head difference. The channel is captured by interface elements located at predefined position under the dam. Current inactive interface elements are collored red and active interface elements that support Poiseuille flow through the channel are colored blue. The flow direction is normal to the equipotential lines as the permeability tensor is isotropic. The active 15 meter long piping channel that drains the aquifer to some extent, this causes a shift in the otherwise symmetrically arranged equipotential lines as shown. DgFlow calculates a critical head of 5.88 meters and a corresponding critical pipe length of 15 meters for this case in which the subsurface has a hydraulic conductivity of 1 m/d. Figure 3.1 shows the critical state for the steady state flow calculation. MSeep obtains a critical head value of 5.41 meters which corresponds well with the outcome of Sellmeijer's rule; 5.44 meters. The difference with the current result can be explained by the difference in implementation of White's criterion on grain equilibrium.

Figure 3.2 presents the critical state for a structure that is supported by a gravel subsurface. For this case the hydraulic conductivity reads 100 m/d. DgFlow calculates a critical head of 1.28 meters and a corresponding critical pipe length of 15 meters. MSeep obtains a critical head value of 1.17 meters which corresponds to the outcome of Sellmeijer's rule.

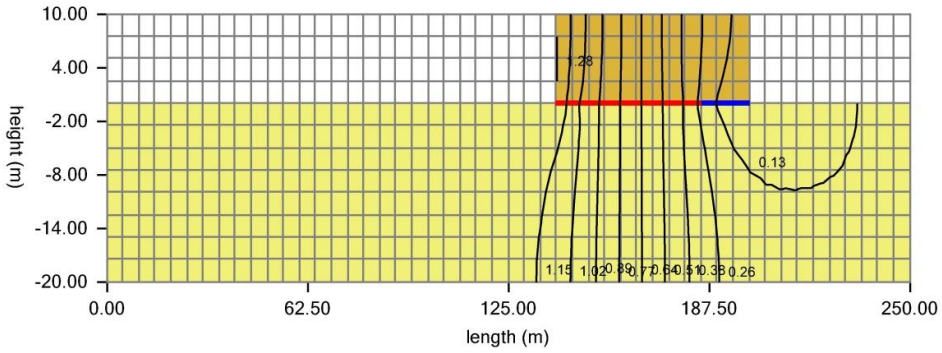

Figure 3.2 Structure on a gravel subsurface.

Figure 3.3 presents the third case, which involves a structure on a sandy subsurface supported by gravel. For this case DgFlow calculates a critical head of 3.23 meter and a critical pipe length of 45 meters for steady-state flow conditions. As a result of the high permeability gravel layer vertical groundwater flow towards the pipe is stronger than for a homogeneous case, which results in an increase in the critical pipe length. MSeep computes a critical height of 3.08 meters for this case. Sellmeijer's rule is not valid for a multilayer subsurface system and can only be used with a single value for the permeability. The gravel case provides a conservative guess for the critical head, whereas the sand case overestimates the critical head.

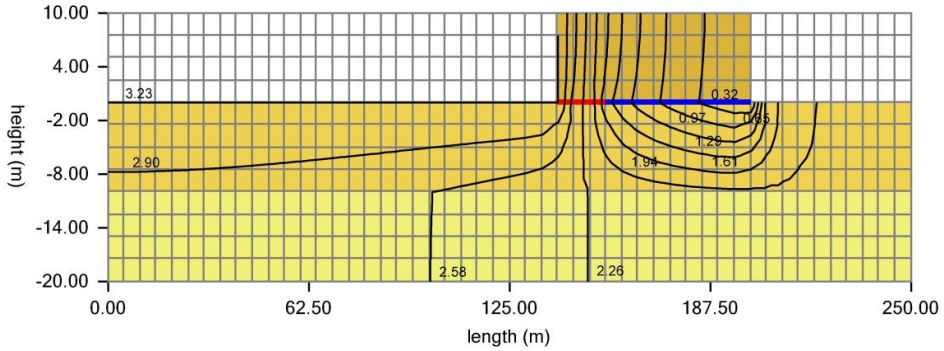

Figure 3.3 Structure on a sandy subsurface supported by gravel.

Figure 3.4 shows the inverse situation of the previous case. Here sand supports a gravel layer. DgFlow calculates a critical head of 1.55 meters and a corresponding critical pipe length of 10 meters. The figure shows this critical state for the steady state groundwater flow situation. MSeep obtains a critical head value of 1.88 meters. This result is closer to the gravel case than the previous two-layered case. The comparison of the gravel on sand and the sand on gravel case illustrate that Sellmeijer's rule with a simple averaged permeability cannot be used as both two-layered cases were constructed out of the same materials, sand and gravel, and lead to different values for the critical head. On the other hand; using the highest value for the permeability can give a very conservative predictions for the critical head, the lowest value provides an unsafe guess.

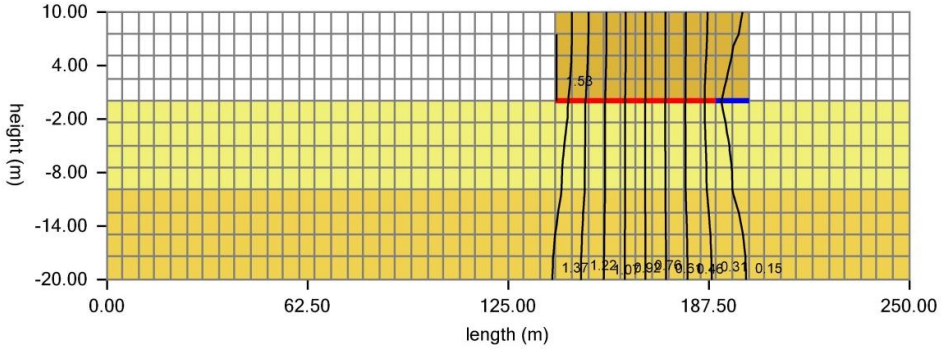

Figure 3.4 Structure on gravel subsurface supported by sand.

The effect of elastic storage in the saturated zone was studied by varying the compressibility of the soil layer and the dike. Table 3.1 presents the results for an increasing compressibility for all materials. The river water level was raised at a rate of 10 meters per 25.5 days.

Case	$\alpha = 10^{-8}$ m^2/N	$\alpha = 10^{-7}$ m^2/N	$\alpha = 10^{-6}$ m^2/N
Sand	5.88	5.15	8.06
Gravel	1.31	1.31	1.24
Sand on gravel	3.26	3.17	3.29
Gravel on sand	1.58	1.55	1.53

Table 3.1 Critical heads for slow river water level variation.

Table 3.1 indicates that a relatively low compressibility of 10^{-8} m^2/N returns values for the critical head that correspond well with the values that were obtained by a steady state analysis. For a compressibility of 10^{-7} m^2/N the pipes start to develop at a higher head difference over the structure due to an increase in elastic storage. However, at a certain moment in time the rate at which the pipes grow numerically is larger than the time needed for the dissipation of groundwater pressures in the vicinity of the pipe. As a result the pipes do not drain their surrounding as much as under steady state conditions and the critical head decreases. The numerical rate is based on an equilibrium consideration of the grains in the channel and the channel's impact on the groundwater pressure field. The transport capacity of the pipe needs to be added to the model in order to get more realistic estimates for the growth rate of the channel in compressible media. For a compressibility of 10^{-6} m^2/N higher values for the critical head were found for the sand case and the sand on gravel case because now the lower rate of groundwater build up dominates over the lower rate of drainage by the pipe. For the gravel case and the gravel on sand case an increase in critical head will be found for even higher values of the compressibility.

The effect of phreatic storage on the critical head was studied by varying the permeability of the embankment. Table 3.2 lists the results for an increasing river water level at a rate of 10 meters per 25.5 days. It can be concluded that a structure with a higher hydraulic conductivity supports more leakage from the subsurface and decreases the pressures at the interface between structure and subsurface. This hampers the development of the pipe.

Case	K = 0.001 m/d	K = 0.01 m/d	K = 0.1 m/d
Sand	6.08	6.66	7.85
Gravel	1.26	1.28	1.28
Sand on gravel	3.24	3.33	3.40
Gravel on sand	1.53	1.53	1.55

Table 3.2 Critical heads for slow river water level variation.

As the outcome of the simulations depends not only on the values of the material parameters but also relates to the rate by which the free water conditions change, next a sea water level signal, where the water level was raised 10 meters in a period of 1.4 days, was imposed.
Table 3.3 and Table 3.4 gather the results for an increase in either compressibility or permeability.

Case	$\alpha = 10^{-8}$ m^2/N	$\alpha = 10^{-7}$ m^2/N	$\alpha = 10^{-6}$ m^2/N
Sand	5.47	> 9	> 9
Gravel	1.28	1.24	1.71
Sand on gravel	2.72	4.46	> 9
Gravel on sand	1.58	1.55	1.96

Table 3.3 Critical heads for fast sea water level variation.

Case	K = 0.001 m/d	K = 0.01 m/d	K = 0.1 m/d
Sand	5.65	7.27	> 9
Gravel	1.28	1.28	1.30
Sand on gravel	3.15	3.31	4.57
Gravel on sand	1.53	1.53	1.59

Table 3.4 Critical heads for fast sea water level variation.

For this case a relative low compressibility of 10^{-8} m^2/N returns values for the critical head that are below the steady state results, although the pipes start to develop at a lower head difference over the structure under steady state conditions. As a consequence of the numerical approach the pipes do not drain their surrounding as much as in the steady state case and groundwater pressures remain relatively high. The combination of a large pressure gradient at a relative large pipe height supports grain transport. An increase of the

compressibility reduces the build up speed of groundwater pressures in the subsurface. This dominates the decreased drainage capacity of the pipe for the sand case and the sand on gravel case and as a result of this higher values for the critical heads are found. As the hydraulic conductivity of gravel is 100 times larger than sand an increase in critical heads is found only if the compressibility is increased even further. Table 3.4 indicates that an increase in the hydraulic conductivity of the structure, which supports phreatic storage, hampers the piping mechanism.

3.2 River dike

Figure 3.5 sows the cross section of the river dike and

Table 3.5 collects the macro-scale material parameters that were imposed. The micro-scale parameters read: particle diameter 0.1 mm; density of the grains of 2.65 10^3 kg/m^3; White's constant of 0.25 and bedding angle of 37 deg.

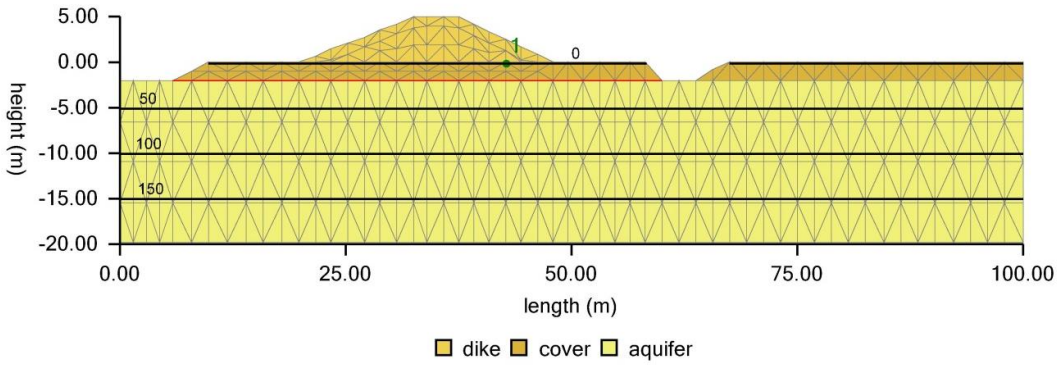

Figure 3.5 River dike.

material	γ^w (kN/m^3)	γ^d (kN/m^3)	α (m^2/kN)	n (-)	K (m/d)
dike	18	17	1.00 10^{-6}	0.50	4.32 10^{-2}
cover	16	16	2.00 10^{-6}	0.60	8.64 10^{-3}
aquifer	20	18	4.00 10^{-6}	0.40	8.64 10^{-0}

Old table

material	γ^w (kN/m^3)	γ^d (kN/m^3)	α (m^2/N)	n (-)	K (m/d)
dike	18	17	1.00 10^{-6}	0.50	4.32 10^{-2}
cover	16	16	5.00 10^{-6}	0.60	8.64 10^{-3}
aquifer	20	18	2.00 10^{-8}	0.40	8.64 10^{-0}

Table 3.5 Material parameters river dike.

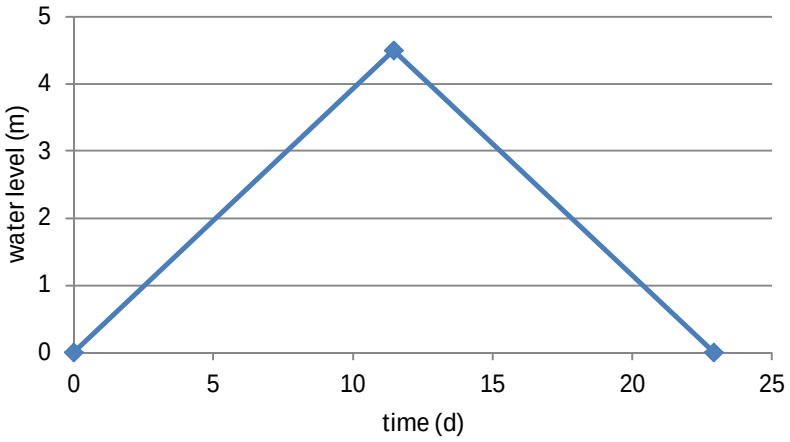

Figure 3.6 Water level variation river dike.

Figure 3.6 shows the river water level in time; at 11.46 days the water level reaches its peak value of 4.5 meters and at 22.92 days the water level is back to its initial value.

DgFlow computes a critical head of 2.95 meters for the river dike under steady state flow conditions. The corresponding critical pipe length is 6.9 meters. For the transient case, given the material parameters of

Table 3.5, again a critical head of 2.95 meters was retrieved. Setting the compressibility of aquifer to 10^{-6} m^2/N, which introduces more elastic storage into the system, does not change the value of the critical head. Also, changing the permeability of both the cover layer and the dike to 0.1 m/d, which increases the phreatic storage of the system, gives a critical head of 2.95 meters.

3.3 Sea defence

Figure 3.7 presents the sea defence that will be studied in this section and Table 3.6 gathers its macro-scale material parameters. The micro-scale parameters read: particle diameter 0.08 mm; density of the grains of 2.65 10^3 kg/m^3; White's constant of 0.25 and bedding angle of 37 deg.

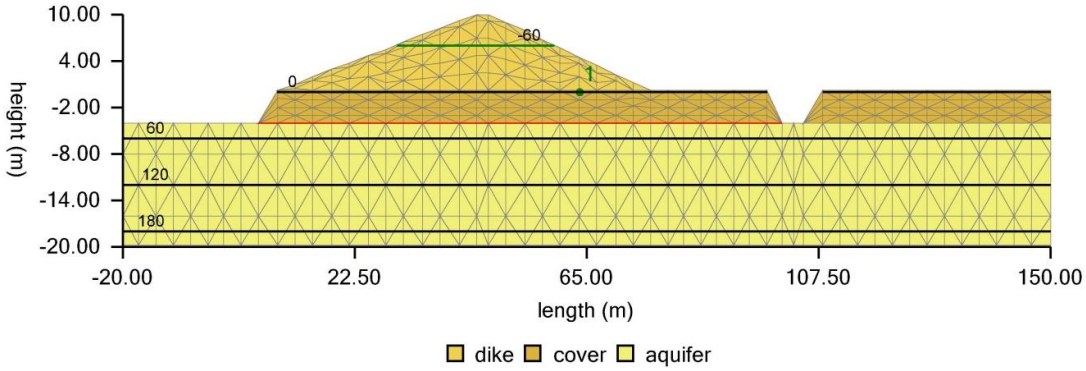

Figure 3.7 Sea defence.

material	γ^w (kg/m^3)	γ^d (kg/m^3)	α (m^2/kN)	n (-)	K (m/d)
dike	20	18	4.00 10^{-8}	0.40	8.64 10^{-0}
cover	16	16	2.00 10^{-6}	0.60	8.64 10^{-3}
aquifer	20	18	4.00 10^{-7}	0.40	8.64 10^{-0}

Old table

material	γ^w (kg/m^3)	γ^d (kg/m^3)	α (m^2/N)	n (-)	K (m/d)
dike	20	18	1.00 10^{-7}	0.40	8.64 10^{-0}
cover	16	16	5.00 10^{-6}	0.60	8.64 10^{-3}
aquifer	20	18	2.00 10^{-8}	0.40	8.64 10^{-0}

Table 3.6 Material parameters sea defence.

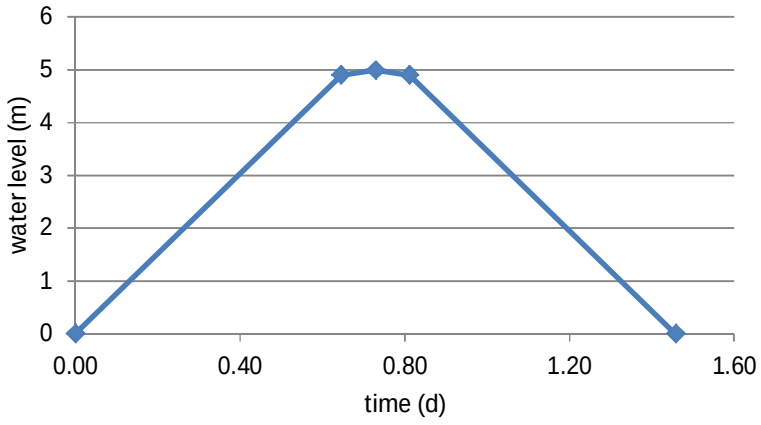

Figure 3.8 Water level variation sea defence.

Figure 3.8 presents the sea water level variation in time, the highest level of 5 meters is found after 0.73 days and after 1.46 days the water level returns to its original state.

For the sea defence case DgFlow computes a critical head of 3.65 meters under steady state flow conditions. The corresponding critical pipe length is 3.0 meters. For the transient case, given the material parameters of Table 3.6, a critical head of 3.87 meters was obtained. Setting the compressibility of aquifer to 10^{-7} m^2/N increases the critical head significantly to 4.92 meters due to additional elastic storage. Setting the permeability of cover layer and the dike to 0.1 m/d increases the critical head to 4.78 meters due to the delay in groundwater pressure build up, which is the result of extra phreatic storage.

4 Conclusions

Groundwater pressures change in time due to time dependent boundary conditions. Elastic storage and phreatic storage delay the response of groundwater pressure build up and affect the piping process. Both porosity and hydraulic conductivity of a structure that is founded on a permeable subsurface determine the amount of phreatic storage in the unsaturated zone of the structure. It can be concluded that a structure with a higher hydraulic conductivity supports more leakage from the subsurface and decreases the pressures at the interface between structure and subsurface. This hampers the development of the pipe. An increase of the structures porosity will also delay the process. Compression of the soil introduces elastic storage, which also delays the build-up of groundwater pressures. However, elastic storage also decreases the drainage of the subsurface by the pipes, which affects the rate at which the pipe grows. This rate can be higher for a system with more elastic storage, which can make the system more sensitive for piping if it dominates the build-up of groundwater pressures. At present the numerical rate at which the pipes grow is based on an equilibrium consideration of the grains in the channel and the channel's impact on the groundwater pressure field. The transport capacity of the pipe needs to be added to the model in order to get more realistic estimates for the growth rate of the channel in compressible media.

The applicability of the model for more realistic cases is investigated by considering a simplified river dike and a sea defense. The river dike case shows that a transient groundwater computation does not provide a different value for the critical head than the value that was obtained by a steady state calculation due to the slow variation of the river water level over time. For the sea defence case DgFlow computes a critical head of 3.65 meters under steady state flow conditions, whereas under transient flow conditions and a set of realistic material parameters a critical head of 3.87 meters was obtained. Setting the compressibility of aquifer to 10^{-7} m^2/N increases the critical head significantly due to additional elastic storage and a value of 4.92 meters was found. Setting the permeability of cover layer and the dike to 0.1 m/d increases the critical head to 4.78 meters due to the delay in groundwater pressure build up, which is the result of extra phreatic storage. Both variations in material parameters are likely to be present along the Dutch coast.

In future a number of well instrumented cases have to be considered in order to quantify the impact of phreatic storage and elastic storage on hampering the piping mechanism.

Notations

a	Height of the erosion channel (m)
d	Particle diameter (m)
d_{70}	70 -particle diameter field (m)
d_{70m}	70-particle diameter lab (m)
D	Aquifer thickness (m)
F_g	Geometry term (-)
F_r	Resistance term (-)
F_s	Scale term (-)
g	Gravitational acceleration (m/s$^{2)}$
H_c	Critical head difference (m)
K	Hydraulic conductivity (m/s)
l	Actual piping length (m)
L	Potential piping length (m)
n	Porosity (-)
N_b	Base functions (-)
p	Pore pressure (N/m^2)
q	Specific discharge (m/s)
$\bar{q}$	Sink term (1/s)
Q	Erosion channel discharge (m^2/s)
W_a	Weighting functions ((-)
y	Elevation level (m)
α	Erosion channel slope (m)
α	Compressibility soil skeleton (m^2/N)
β	Compressibility pore water (m^2/N)$^{)}$
γ^p	Submerged unit weight (N/m^3)
γ^w	Unit weight water (N/m^3)
Γ	Flow domain boundary (m)
η	White's constant (-)
ϑ	Bedding angle (deg)

κ_{ij}	Intrinsic permeability (m^2)
λ	Lamè's constant (N/m^2)
μ	Dynamic viscosity water (Ns/m^2)
ν	Lamè's constant (N/m^2)
ρ^w	Density water (kg/m^3)
ϕ	Hydraulic head (m)
Ω	Flow domain (m^2)

Bibliography

Aziz, K. and A. Settari, 2002. Petroleum Reservoir Simulation. Blitzprint Ltd., Calgary, Alberta.

De Wit, J. M., 1984. Onderzoek Zandmeevoerende Wellen - Rapportage Modelproeven, vol. 220887/10. Grondmechanica Delft.

Hanses U (1985) Zur Mechanik der Entwicklung von Erosionskanälen in geschichtetem Untergrund unter Stauanlagen. Dissertation Grundbauinstitut der Technischen Universität Berlin, Germany.

Huyakorn, P. S. and G. F. Pinder, 1983. Computational Methods in Subsurface Flow. Academic Press.

Lane, E. W., 1935. “Security from Under-Seepage-Masonry Dams on Earth Foundations.” Transactions of the American Society of Civil Engineers 100 (1): 1235–1272.

Sellmeijer, J. B., 1988. On the mechanism of piping under impervious structures. Ph.D. thesis, Delft University of Technology, Delft, The Netherlands.

Sellmeijer, J. B., J. Lopez de la Cruz, V. M. Van Beek and J. G. Knoeff, 2011. “Fine-tuning of the piping model through small-scale, medium-scale and IJkdijk experiments.” European Journal of Environmental and Civil Engineering 15 (8): 1139–1154.

Van Beek, V.M., Van Essen, H., Bezuijen, A., 2014a, Developments in modeling of backward erosion piping, to be published

Van Beek, V.M., Vandenboer, K., Bezuijen, A., 2014b, Infuence of sand type on pipe development in small- and medium-scale experiments, ICE7.

Van Esch, J. M., J. B. Sellmeijer and D. Stolle, 2013a. “Modeling Transient Groundwater Flow and Piping under Dikes and Dams.” In G. Pande and S. Pietruszczak, eds., Computational Geomechanics (ComGeo III). Taylor & Francis Group.

Van Esch, J. M., J. A. M. Teunissen and D. Stolle, 2013b. “Modeling Transient Groundwater Flow under Dikes and Dams for Stability Assessment.” In G. Pande and S. Pietruszczak, eds., Computational Geomechanics (ComGeo III). Taylor & Francis Group.

Vogel, T., M. T. Van Genuchten and M. Cislerova, 2001. “Effect of the Shape of the Soil Hydraulic Functions Near Saturation on Variably-Saturated Flow Predictions.” Advances in Water Resources 24: 133–144.

White, C., 1940. “The equilibrium of grains on the bed of a stream.” Proceedings Royal Society (174A): 322–338.

Wolfs, T. F., 2002. Performance of Levee Underseepage Controls: A Critical Review, vol. ERDC/GSLTR-02-19. Michigan State University.